Effect of pH, Temperature and Shear on the Structure-Property Relationship of Lamellar Hydrogels from Microbial Glucolipids Probed by in-situ Rheo-SAXS

Ghazi Ben Messaoud, Patrick Le Griel, Daniel Hermida-Merino, Niki Baccile

Effect of pH, Temperature and Shear on the Structure-Property Relationship of Lamellar Hydrogels from Microbial Glucolipids Probed by *in-situ* Rheo-SAXS

Ghazi Ben Messaoud,[1,†] Patrick Le Griel,[1] Daniel Hermida-Merino,[2] Niki Baccile[1,*]

[1] Sorbonne Université, Centre National de la Recherche Scientifique, Laboratoire de Chimie de la Matière Condensée de Paris, LCMCP, F-75005 Paris, France

[2] Netherlands Organisation for Scientific Research (NWO), DUBBLE@ESRF BP CS40220, 38043 Grenoble, France

*Correspondence to: Dr. Niki Baccile, niki.baccile@sorbonne-universite.fr, Phone: 00 33 1 44 27 56 77

† Current address: DWI- Leibniz Institute for Interactive Materials, Forckenbeckstrasse 50, 52056, Aachen, Germany

DOI: 10.1039/c9sm02494h

Abstract

Lipid lamellar hydrogels are a class of soft materials composed of a defectuous lipid lamellar phase, where defects are classically stabilized by polymers or surfactants inclusions in the lipid membrane. We have recently shown that bolaform microbial glucolipids, composed of a single glucose headgroup and a C18:0 fatty acid, with the carboxylic acid located at the opposite of glucose, spontaneously form lamellar hydrogels at room temperature below pH 8. In this work, we combine rheology with small angle x-ray scattering (SAXS), rheo-SAXS, to correlate, *in-situ*, the structural and mechanical properties of microbial glycolipid lamellar hydrogels upon application of three different stimuli: pH, temperature and shear rate. In all cases we find unusual structural features of the lamellar phase if compared to classical phospholipid lamellar structures: reducing pH from alkaline to acidic induces a sol-to-gel transition during which the increasing elastic modulus is associated to an oscillatory evolution of lamellar $d_{(100)}$ spacing; temperature above T_m and increasing shear induce the formation of spherulitic crumpled domains, instead of a classically-expected lamellar-to-vesicle or lamellar-to-onion phase transitions.

Introduction

2D and 3D soft self-assembled materials are usually obtained from stimuli-responsive peptides, proteins or lipids,[1–4] and they attract a large interest for the increasing number of applications[5] such as protective coating for cells,[6] regenerative medicine,[7] lab-on-a-membrane prototyping,[8] self-healing materials.[9] Lipids, which can self-assemble into a variety of soft structures,[10] are particularly interesting systems because of the possibility to form isotropic (entangled fibers) or anisotropic (lamellar) gels,[11] characterized by tunable mechanical properties.

Lipid lamellar hydrogels (LH) at concentrations below 10 wt% were discovered more than twenty years ago and they are much less common systems if compared to self-assembled fibrillar network hydrogels.[12–14] They were observed in a phospholipid L_α phase stabilized by a polymer-grafted lipid.[15] Since then, this class of soft materials was mainly reported in phospholipid lamellar phase stabilized by a polymer,[16] or by combining a lamellar phase with a gelator.[17,18] The first polymer-free LH, based on surfactant mixtures or lipid/surfactants, were only reported in 2014.[19,20] The elastic properties in LH depend on the amount of defects in the bilayer membrane,[15] thus making the control over their mechanical properties very hard. Despite this drawback, LH constitute an opportunity in preparing new 2D and 3D materials.[19,21]

In a recent work,[22] we have shown the hydrogel-formation properties of a new, biobased, lipid composed of a single glucose unit covalently linked via an acetal bond to a C18:0 fatty acid (stearic acid), leaving the carboxylic acid free at the opposite end of the glucose moiety (**Figure 1a**). This molecule, entirely derived from glucose and vegetable oil, fermented and produced in large amounts (~0.5 $gL^{-1}h^{-1}$) by the modified yeast *S. bombicola ΔugtB1*,[23] forms stable hydrogels above lipid concentration of 1 wt% by a simple pH adjustment between 5 and 7.5 and at ionic strength above ~50 mM.[22] **Figure 1a** summarizes

the reversible micelle-to-membrane formation of G-C18:0 induced by pH and where the membrane structure is identified as an interdigitated arrangement of the molecule, characterized by COOH and COO^- groups. **Figure 1b** shows a typical G-C18:0 hydrogel, best described as a multiscale assembly of defectuous lamellar domains.[22]

G-C18:0 is part of the so-called biological amphiphile, or biosurfactant, family, a class of molecules exclusively obtained by fermentation of vegetable oils and largely studied for their interest in developing new biodegradable surfactants with additional interesting antimicrobial, emulsifying or remediation properties, just to cite some.[24,25] If the self-assembly of biological amphiphiles has become an important topic in past ten years,[26,27] their gelation has received much less attention[28–31] and the structure-properties relationships were only reported for fibrillar sophorolipid hydrogels.[30,31] In fact, considering the overall rarity of lamellar hydrogels, the studies investigating the structure-property relationship in this class of soft materials are seldom published.[32,33]

The present work shows a microstructural characterization of lamellar G-C18:0 hydrogels by an *in-situ* coupling of rheology and small angle X-ray scattering (SAXS). We explore the effect of pH variation from alkaline to acidic, thus exploring the micellar-to-lamellar phase transition and in particular how the evolution of the lipid structural parameters can be associated to the increasing elastic properties of the gel. We also investigate the effect of temperature and shear on the elastic properties and, in particular, on the microstructure of the lipid assembly. Surprisingly, we find that: the increasing elastic properties observed during the pH-induced micelle-to-lamellar transition are associated to an oscillatory behavior of the lamellar $d_{(100)}$ spacing and its stabilization below 20 nm; temperature and shear rate promote the formation of what seems to be a crumpled spherulitic phase instead of a more classical vesicle or onion phase. These data do not only provide a better understanding of the specific glycolipid hydrogel, but, by presenting unexpected results with respect to the broader

literature of phospholipid lamellar gels, they open new perspectives in the broader field of lamellar hydrogels and lamellar phases.

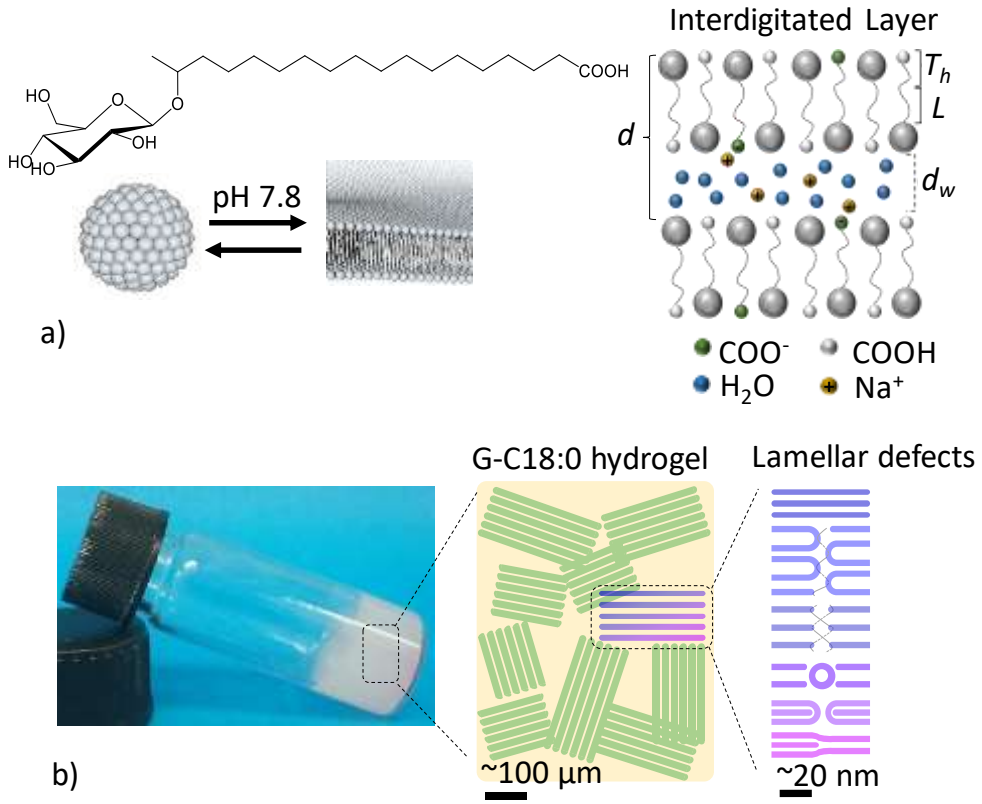

Figure 1 – a) Molecular structure of microbial (derived from *S. bombicola ΔugtB1*) glucolipid G-C18:0 (17-L-[(β-D-glucopyranosyl)oxy]-cis-9-octadecenoic acid) and its pH-dependent phase behavior at room temperature: a micelle-rich phase occurs at pH above 7.8 and a lamellar phase forms at pH below 7.8.[34,35] **Each lamella is composed of an interdigitated lipid layer where T_h is the thickness of the hydrophilic region, L is the length of the hydrophobic region, d_w is the interlamellar water thickness and d the lamellar period, $d_{(100)}$. b) Typical image of a G-C18:0 hydrogel at room temperature and its structure, composed of defectuous (displocations, disclinations, spherulite inclusions as well as screw dislocations) lamellar domains (tens to hundred of microns).**[22] **Each membrane is composed of an interdigitated layer of G-C18:0 molecules as in a).**[22,34,35]

Materials and Methods

Chemicals. The microbial monunstaurated glucolipid G-C18:1 was produced at a production rate of ~ 0.5 $gL^{-1}h^{-1}$ in a bioreactor system using a modified strain (*ΔugtB1*) of the yeast

Starmerella bombicola[23] and according to the experimental conditions described in ref.[34]. The fully saturated G-C18:0 (M_w = 462.6 g.mol^{-1}), used in this work, is obtained as a > 95% pure molecule from GC18:1 by a catalytic hydrogenation reaction, described in ref. [34]. The NMR, HPLC and LC-MS analyses of G-C18:0 can be found in ref. [34]. Glucono-δ-lactone (GDL, M_w = 178.14 g.mol^{-1}) is purchased from Sigma Aldrich. 18:1 Liss Rhod PE (M_w= 1301.7 g.mol^{-1}, λ_{abs}= 560 nm, λ_{em}= 583 nm), 1,2-dioleoyl-sn-glycero-3-phosphoethanolamine-N-(lissamine rhodamine B sulfonyl) (ammonium salt), is purchased by Avanti® Polar, Inc.

Preparation of G-C18:0 hydrogels. A given amount of G-C18:0 (in wt%) is first dispersed in water (volume is gnerally 1 mL) and sonicated during 5 to 10 minutes to break the aggregated powder. The pH of the solution is then raised under stirring with μL amounts (generally between 2 and 30, according to the amount of sample) of 5 M NaOH until pH ~9-10 is reached. The solution becomes a partially clear sol at pH > 8, as discussed in a previous work.[34] The sol-to-gel transition is then studied during *in-situ* acidification using glucono-δ-lactone (GDL). A given amount of GDL is weighted in a vial, to which the alkaline G-C18:0 solution is added. Mixing is achieved by vortexing for approximately 10 to 20 seconds and the sample is allowed to stand still (no additional vortexing, sonication, stirring) with gelation taking place at room temperature. For the rheo-SAXS experiments, the G-C18:0 solution at basic pH is immediately placed in the couette cell after mixing with GDL. A constant GDL:G-C18:0 molar ratio of 1.08:1 is selected. Indeed, to prepare G-C18:0 solutions of 10, 25, 50 and 100 mg.mL^{-1}, we respectively employ concentrations of GDL of 3.56, 8.9, 17.8 and 35.6 mg.mL^{-1}. Unless otherwise stated, room temperature (RT) is taken as 23 ± 2 °C.

Rheo-SAXS. Experiments coupling rheology and SAXS are performed at the DUBBLE BM26B beamline at the ESRF synchrotron facility (Grenoble, France)[36,37] during the SC4778

run, using a beam energy of 12.65 KeV and a sample-to-detector distance of 3.23 m. Silver behenate ($d_{(001)}$ = 58.38 Å) is used as q-calibration standard. The signal of the Pilatus 1M 2D detector (172 x 172 μm pixel size), used to record the data, is integrated azimuthally with PyFAI software to obtain the *I(q)* spectrum ($q = {4\pi \sin\theta}/{\lambda}$, where 2θ is the scattering angle) after masking systematically wrong pixels and the beam stop shadow. A MCR 501 rheometer (Anton Paar, Graz, Austria) equipped with a Couette polycarbonate cell (gap 1 mm) is coupled to the beamline and controlled through an external computer in the experimental hutch using the Rheoplus/32 V3.62 software. The experiments are performed in a radial configuration, where the X-ray beam is aligned along the center of the Couette cell. The rheology and SAXS acquisitions are synchronized manually with an estimated time error of less than 5 s. Due to standard security procedures, the first rheo-SAXS experimental point is systematically acquired with a delay of about 3-4 minutes. The experimental setup is shown on **Figure S 1**. Data are not scaled to absolute intensity.

Analysis of the SAXS data. The lamellar phase formed by the G-C18:0 glucolipid was previously characterized by SAXS and it was described by two symmetrical hydrophilic regions, containing the glucose and COOH moieties, separated by an interdigitated layer of the C18 chain.[34] The corresponding structural parameters, illustrated in **Figure 1a**, are: thickness of the hydrophilic region: T_h= 1.4 nm; length of the hydrophobic core: L= 0.8 nm. The total thickness of the bilayer is then ($2T_h + L$)= 3.6 nm, where the error coming from the fitting procedure of the corresponding SAXS data is estimated to about ±10%. Unless otherwise stated, we use these values to characterize the lamellae.

The rheo-SAXS experiments performed in this work are analyzed in a similar way using the SasView software (version 3.1.2): we combined a core-shell bicelle form factor model,[38] as in ref. [34], with a Lorentzian peak function,[39] to account for the presence of the broad low-q

correlation peak. For the core-shell bicelle form factor, we use a large value of the bicelle radius (R= 100 nm), thus mimicking a large flat object, analogous to a bilayer. The rim radius is set to zero. The scattering length densities (SLD) are adjusted as in ref.[34]: the SLD value of H_20 is $9.4 \cdot 10^{-4}$ nm^{-2} while the core SLD is set to $8.3 \cdot 10^{-4}$ nm^{-2}, which represents a typical value for an aliphatic chain. The SLD of the hydrophilic region is set $10.9 \cdot 10^{-4}$ nm^{-2}. However, due to the fact that we do not employ an absolute scale, the SLD values cannot be quantitatively exploited and the intensity level is adjusted through the scaling factor given in the model. In the end, T_h, L and the scaling factor are the only free variables of the bicelle model. The Lorentzian peak is controlled by the full width at half maximum, the peak position and scaling factor, which are qualitatively estimated at the beginning of the fit and allowed to vary for refinement.

Rheology. In-lab rheology experiments are carried out using a MCR 302 rheometer (Anton Paar, Graz, Austria) with a sand-blasted plate-and-plate geometry (diameter 25 mm, gap = 0.5 mm). The rheometer is equipped with a Peltier temperature system, which allows accurate control of the temperature by the stainless steel lower plate, while water evaporation is minimized with a solvent trap during the measurements. Except for thermal annealing experiments, all rheological characterizations are conducted at 25 °C, unless otherwise mentioned.

- *Oscillatory rheology*. Frequency time sweep experiments are performed to monitor the gelation kinetic of the G-C18:0 samples by slow acidification. Briefly, the glucolipid alkaline solution is mixed with the appropriate amount of GDL and the final mixture is vortexed for 20 seconds and immediately loaded on the bottom plate. Dynamic oscillatory time sweep experiments are then performed by applying a constant angular frequency (ω = 6.28 rad·s^{-1}) and a shear strain (γ) within the linear viscoelastic regime

(LVER, 0.05 - 0.1 %) and data are collected during 720 minutes at 25 °C. A delay of 3-5 minutes occurs between the moment of mixing and the beginning of the measurement. To monitor the gelation of the G-C18:0 upon thermal annealing, the elastic (G') and viscous (G'') moduli are recorded during temperature heating ramps from 20 to 70 °C at a rate of 10 °C/min. The sample is initially vortexed, then loaded and held at 70 °C for 10 min and then cooled from 70 to 25 °C at a rate of 10 °C/min and finally held at 25°C during two hours. These temperature variation experiments are performed using an oscillation angular frequency of ω= 6.28 rad·s^{-1} and a strain of γ = 0.05%. Afterward, an angular frequency sweep (100 – 0.01 rad·s^{-1}) is performed using a shear strain, γ= 0.05%, within the LVER.

- *Shear viscosity*. Steady-shear viscosity is studied using the plate-plate geometry by increasing the shear rate ($\dot{\gamma}$) from 10^{-3} to 10^{3} s^{-1}.

Nuclear Magnetic Resonance (NMR): time-resolved ^{1}H solution NMR experiments are acquired on a Bruker Avance III 300 spectrometer using a 5 mm ^{1}H-X BBFO probe. Number of transient is 16 with 5 s recycling delay. Experiments are carried out as follows: a 5 wt% solution prepared in D_2O (500 μL) at pD ~11 is mixed with 100 mM GDL at RT, introduced in a standard 5 mm NMR tube and immediately inserted in the NMR spectrometer. The entire process requires about 6 min from the moment of mixing to first acquired ^{1}H NMR scan. Absolute values of the peak area as a function of time are obtained using the *integration* and *relaxation* moduli of the Topspin™ 3.5 pl7 version of the software. We have observed that phasing problems due to change in pH may affect the peak of residual H_2O. Since this is the most intense peak, poor phasing can affect the baseline in the vicinity of the sugar C<u>H</u> region between 3 ppm and 4.5 ppm. This unavoidable fact strongly affects the actual value of the peak area. For this reason, we mainly present the time-resolved evolution of the aliphatic peak

area, contained between 0 ppm and 3 ppm. Peak area normalization is performed with respect to the spectrum recorded before adding GDL, when the entire G-C18:0 population is detected in the micellar phase. The integrated signal corresponds to the molar fraction of G-C18:0 in the soluble micellar phase, defined X_M. The fraction of G-C18:0 in the lamellar phase, X_L, is simply obtained by $X_L = 1 - X_M$, according to the reasonable assumption that the mobility in the lamellar environment is so slow that becomes undetected by NMR. This hypothesis is commonly verified in many self-assembled hydrogels.[40,41]

Confocal Laser Scanning Microscopy (CLSM): CLSM is performed with a LeicaSP8 Tandem Confocal system. Samples are excited with the dye specific wavelength (561 nm) and the emission is detected between 580 and 620 nm using a photomultiplier tube (PMT) detector. CLSM images are analyzed using Fiji (Fiji is just ImageJ)[42] and 3D construction is performed using the 3D Stack mode of Fiji. Temperature variation (T= 50°C) is performed with temperature controller modulus of the microscope. The hydrogel ($C_{G\text{-}C18:0}$= 2.5 wt%, pH 6) is prepared following the general method described above. A volume of 4 µL of an ethanolic solution of 18:1 Liss Rhod PE (C= 53 mg/mL) is added to 1.5 mL of the hydrogel to reach an approximate molar ratio of G-C18:0/Liss of 500. Liss is a water insoluble, rhodamine-containing, lipid and it is largely used to mark lipid bilayers. It is generally considered not to interfere with the bilayer assembly at Lipid/Liss ratio above 200.[43] We did not observe any variation in the gel physical aspect after addition of Liss.

Light Microscopy. Images of G-C18:0 samples after shear are acquired in a differential interference contrast mode (DIC-M) using a Zeiss AxioImager D1 microscope.

Cryogenic Transmission Electron Microscopy (Cryo-TEM). These experiments were carried out on an FEI Tecnai 120 twin microscope operating at 120 kV equipped with a Gatan Orius CCD numeric camera. The sample holder was a Gatan Cryoholder (Gatan 626DH, Gatan). Digital Micrograph software was used for image acquisition. Cryofixation was done on a homemade cryofixation device. The solutions were deposited on a glow-discharged holey carbon coated TEM copper grid (Quantifoil R2/2, Germany). Excess solution was removed and the grid was immediately plunged into liquid ethane at −180 °C before transferring them into liquid nitrogen. All grids were kept at liquid nitrogen temperature throughout all experimentation.

Results and discussion

The development of a new class of single-molecule lamellar hydrogels based on the self-assembly of G-C18:0 glucolipids[22] requires the better understanding of the impact of three independent stimuli (pH, temperature and shear rate) on the gel mechanical and structural properties. G-C18:0 contains a free-standing COOH group, sensitive to pH variations, and its T_m is of 37°C, close to room temperature.[22] In addition, G-C18:0 hydrogels were shown to have shear-thinning properties, thus opening their possible use in a broad set of applications in cosmetics, food science or biomedical field. All in all, pH, temperature and shear all affect the sol-to-gel transition under different conditions, and, in order to better understand their effect on both the phase behavior and the elastic properties, we perform an *in-situ* rheo-SAXS (apparatus shown in **Figure S 1)** combined with cryo-TEM and optical microscopy. The effect of each parameter is discussed hereafter in the following order: pH, temperature and shear.

Effect of pH. G-C18:0 has an apparent pKa of 8.4 ± 0.1[22] and micelle-to-lamellar transition pH of about 7.8, below which the ionization degree is estimated to < 0.2.[22,34,35]

Above pH 8, the solution is fluid, while below pH 8 the viscosity increases. Increasing and decreasing pH respectively promote gel-to-sol and sol-to-gel transitions and in the following we explore the latter on the mechanical and structural properties of the gel.

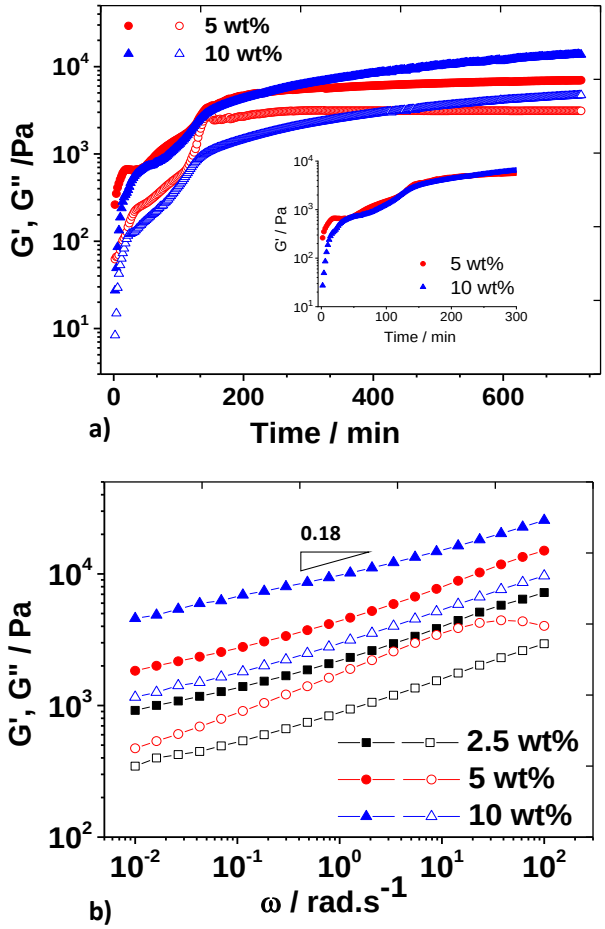

Figure 2 – a) Sol-to-gel transition promoted by pH (use of GDL) through time-resolved *G´* (full symbols) *G´´* (open symbols) as a function of G-C18:0 concentration (initial pH 11, ω= 6.28 rad·s^{-1}, γ = 0.1%, Normal Force = 0 N, initial gap 1 mm), plate-plate geometry (25 mm), [GDL]= 100 mM at $C_{G\text{-}C18:0}$= 5 and 10 wt%). b) *G´*(ω) (full symbols) and *G´´*(ω) (open symbols) measured for 2.5 wt% < $C_{GC\text{-}18:0}$ < 10 wt% after 720 min (γ= 0.1 %) from addition of GDL (initial pH 8.1).

Approaching the sol-to-gel transition by manual addition of HCl to a fluid G-C18:0 sample above pH 8 is a possible but tedious, uncontrolled, process due to local formation of gelly aggregates. For this reason, we employ glucono-δ-lactone (GDL)[44] to reduce pH in a more homogeneous way. GDL, which hydrolyzes into gluconic acid, is an acidifier commonly

used to prepare strong low-molecular weight gels in a homogeneous way and without interfering with the self-assembly process.[41] **Figure 2a** shows the evolution of *G´* and *G´´* with time for two typical G-C18:0 samples of 5 wt% and 10 wt%, initially at pH 11 and with the final pH after 600 min of about 4.5. Both experiments are characterized by an initial steep increase in the moduli and which we speculate to be attributed to a micellar-to-lamellar phase transition on the basis of our previous work at concentration below 0.5 wt%;[35] this aspect will be confirmed by rheo-SAXS experiments below. A short plateau between 500 Pa and 700 Pa, indicatively below 50 min, and a second increase of the moduli between about 100 min and 200 min, probably hide a series of phenomena: increase in the number of lamellar structures followed by structural modification like lateral growth, local bending, spatial reorganization and interfacial rearrangements. Beyond about 200 min, the monotonous increase in the moduli up to 650 min, and reaching 10^4 Pa, suggests a more homogeneous bulk gelation phenomenon, most likely due to proliferation of defects, of which this material is rich.[22] Despite such a simple description, and which partly seem to be comparable to the evolution of the mechanical properties for other low-molecular weight gelators induced by pH,[45] one should still note an oscillation of *G´* and *G´´* below 200 min. For this reason, we have studied the time evolution of the viscoelastic properties during the pH-induced sol-to-gel transition by *in-situ* rheo-SAXS experiments.

The *G´* and *G´´*, as well as the pH evolutions, are plot against time in **Figure 3a**, which shows a rapid increase of *G´* and *G´´* within the initial 10 min, corresponding to a sharp pH drop. A pseudo-plateau is observed between ~50 and ~200 min reaching about 100 Pa; a second increase in the moduli occurs before the last region above 300 min. This behaviour is very similar to what we find in **Figure 2a**, except for the double cross over between *G´* and *G´´* and where *G´´*> *G´* between 10 min and 250 min. At the moment, we attribute this behaviour to possible shrinking phenomena during the sol-to-gel transition in relationship to

the use of a couette cell with fixed gap in the rheo-SAXS experiment, while experiments in **Figure 2a** are obtained using a plate-plate geometry with imposed zero normal force. Similar phenomena are described elsewhere.[46]

After formation of the gels ($G' > G''$), and at sufficiently long lag time, the moduli are practically constant (**Figure 3a**), and G' can reach values up to 10^4 Pa. This value is one order of magnitude higher than the classical G' reported for lamellar hydrogels below 10 wt%,[19,33,47] and two to three orders of magnitude higher than G' reported for onion (5 wt%, L'_α, $G' \sim$ 10 Pa) and onion+lamellar (15 wt%, L'_α+L_α, $G' \sim 10^2$ Pa) phases found for nonionic surfactants in water.[48] $G'(\omega)$ and $G''(\omega)$ (**Figure 2b**) recorded on the gel after the pH-driven sol-to-gel transition display the same dependency with the angular frequency observed for as-prepared hydrogels at constant pH and given ionic strength.[22] Such similarity shows that the method of preparation does not affect the nature of the gel but only the elastic modulus at plateau. In summary, lamellar hydrogels can be prepared either by reducing the pH from basic to acidic or by simply dispersing the G-C18:0 powder in water and adjusting the pH between 5 and 7.5 and ionic strength.

Finally, we carried out ^{1}H solution NMR experiments in solution to probe the amount of glucolipid in the gel state. NMR is highly sensitive to molecular mobility, because the spectral linewidth is inversely proportional to the molecular mobility; in solution, only fast-tumbling molecules can be detected by NMR. Applied to a sol-to-gel transition in a molecular system, solution NMR will only detect the molecule in the sol (here, micellar) environment but not in the gel (here, lamellar) phase. This approach was long used to quantify the extent of gelation in low-molecular weight gelator systems.[41,49,50] **Figure S 2a** shows the evolution of the molecular fraction of G-C18:0 during the pH-induced sol-to-gel transition, where X_M and X_L are respectively the micellar and lamellar (X_L= 1 - X_M) fractions. The evolution of the corresponding spectral signature of G-C18:0 (interval $3 < \delta/\text{ppm} < 0.8$, corresponding to the

C18 chain) from the micellar to the lamellar environments is shown in **Figure S 2b**. We find that the micellar-to-lamellar phase transition is practically quantitative and stable over time, as 95% of G-C18:0 is in the lamellar phase.

Figure 4a presents representative SAXS patterns recorded *in-situ* during the sol-to-gel transition (**Figure 3a**) from pH 8 to pH 5. The SAXS profiles below 15 min are typical for a micellar phase, of which the form factor was largely analyzed for the G-C18:0 in a previous work.[35] Below pH 8, the oscillation at $q > 1$ nm^{-1} and the broad peaks (indicated by symbols ° and ¤) at $q < 1$ nm^{-1} respectively characterize the form factor of the lipid layer and lamellar period, *d*, similarly to the SAXS and SANS profiles of the same material recorded at pH below 7.[22] The structural transition from micelles to lamellae when pH is reduced from alkaline to acidic confirms *in-toto* the finding of our previous studies[34,35] and for this reason the analysis of this particular aspect of the *in-situ* rheo-SAXS data will not be repeated here, where we will only address the evolution of the lamellar structure in relationship to the hydrogel mechanical properties.

The typical numerical fits of the SAXS data corresponding to selected profiles during the pH-induced sol-to-gel transition are shown in **Figure 4b** and the detailed fitting strategy is given in the materials and method section. The time-resolved fits give access to the structural parameter of the lamellar phase, namely the thickness of the hydrophilic, T_h, and hydrophobic, L, regions, and the lamellar period, d. Considering that $d = d_w + (2T_h + L)$, where $(2T_h + L)$ is full membrane thickness and d_w is the interlamellar water layer thickness, d_w (**Figure 1a**), it is easily possible to determine d_w from T_h, L and d. The evolution of d_w and $(2T_h + L)$ with time during the sol-to-gel transition is shown in **Figure 3b**, which also shows the corresponding evolution of G'. As a general comment, the lamellar period, *d*, significantly evolves over time; decorrelation of d_w from $(2T_h + L)$, as shown in **Figure 3b**, indicates that the source of such variation mainly depends on the water later thickness, rather than the membrane

thickness. The slight (15%) increase between 0 and 300 min of the latter can be safely considered as practically constant within the error of the fit (10%) and in comparison to d_w, undergoing a 50% variation over the same time period. The average value of the membrane thickness is about 3.5 ± 0.25 nm, in very good agreement with the thickness value found in previous studies and characteristics of an interdigitated arrangement of the G-C18:0 lipids.[22,34,35] Considering the poor relevance in terms of the evolution of the membrane thickness during the sol-to-gel transition, we will only discuss, in the following, the evolution of d_w.

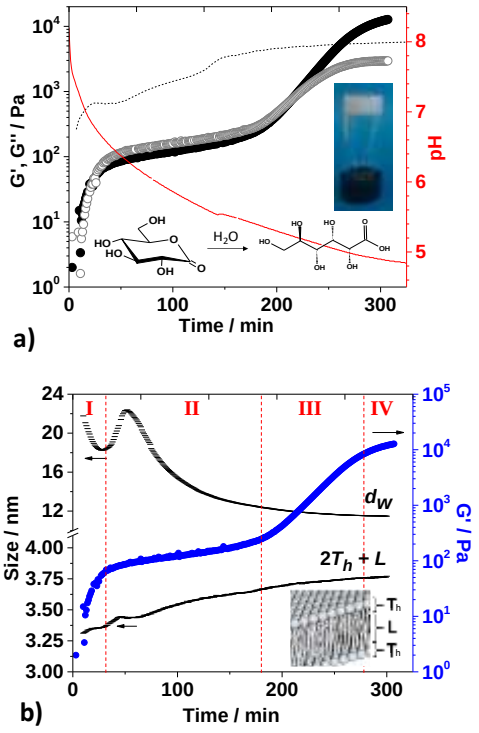

Figure 3 – *In-situ* rheo-SAXS experiments. a) Rheology. Time evolution of *G´* (full symbols), *G´´* (open symbols) (*ω*= 6.28 rad·s^{-1}, *γ*= 0.1%, constant gap 1 mm, couette cell geometry) and pH (red curve). The *G´´*> *G´* at *t*> 50 min is an artifact most likely due to the constant gap of the couette cell, because no multiple cross-over exists in the plate-plate geometry with constant normal force (Figure 2a). The dotted line represents the *G´* at 5 wt% presented in Figure 2a and collected under constant normal force. b) SAXS. Time evolution of interlamellar water layer, d_w, and membrane, ($2T_h + L$), thickness derived from SAXS data analysis of rheo-SAXS data in Figure 4. Blue symbols correspond to *G´*.

The combined viscoelastic and structural properties of the lamellar hydrogel during the sol-to-gel transition can be divided into four time domains (TD) (**Figure 3b**):

TD-I) t< 40 min: sharp increase of both moduli up to 10^2 Pa, pH reaches ~6.5 and d_w decreases from 22 nm to 18 nm: TD-I is characterized by an increase in the concentration of lamellae per unit volume due to the completion (t ~40 min) of the micelle-lamellar transition probed by NMR (**Figure S 2**);

TD-II) *50 < t/min < 170* is characterized by a pseudo-plateau, both moduli slowly increase with time, d_w increases back to 22 nm before dropping towards 12 nm. To the best of our knowledge, the oscillating behavior of d_w was not reported before on any of the lamellar hydrogels studied in the literature. If the exact origin of such oscillation is unclear, it could either be related to fluctuations in the charge density of the membrane or to variation in the osmotic pressure. More comments on this point are given below;

TD-III) *200<t/min<300*: sharp increase of *G´* and *G´´*;

TD-IV) *t>300 min*: stabilization of *G´* and *G´´*, with d_w~12 nm: lowering of pH reduces the charge density (less COO^- groups) in the IL, resulting in closer lamellae.

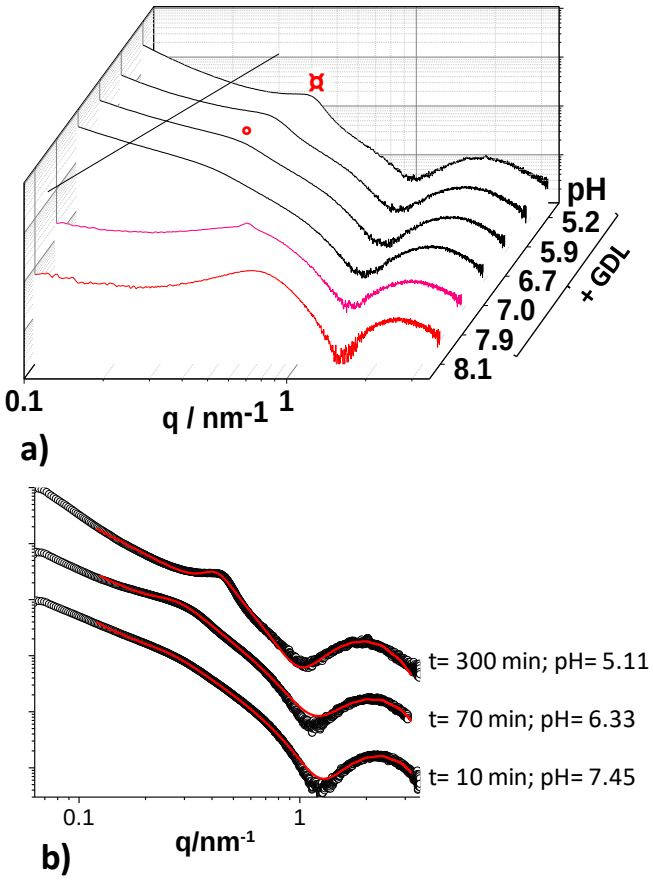

Figure 4 – a) pH-driven sol-to-gel transition probed using rheo-SAXS ($C_{G\text{-}C18:0}$= 5 wt%, initial pH 8.1, pH is reduced using GDL, with [GDL]= 100 mM). Selected SAXS profiles of the rheo-SAXS experiment. Symbols ° and ¤ indicate the broad peak attributed to the lamellar period, *d* (Figure 1a).[22] b) Typical fits of selected SAXS profiles from (a). The fitting strategy is described in the materials and methods section of the paper.

The unusual rheological sol-to-gel transition is related to the gelation mechanism of the G-C18:0 hydrogels. The addition of GDL induces an initial fast increase in the mechanical properties, followed by a slow pH decrease of the solution. As a first consequence, a transition from a micellar to a lamellar phase occurs, thus leading to an increase of the viscosity as well as of the elastic modulus, which remains constant at around 100 Pa. NMR experiments suggest that the increase in the elastic modulus can be associated to the increasing concentration of the lamellar structures. However, the oscillating evolution of the

lamellar period, *d*, shows that other concomitant phenomena may occur, such as lateral growth, bending, spatial reorganization and interfacial rearrangements of the lamellae. Unfortunately, these phenomena are difficult to probe in a direct manner. Both moduli eventually increase until the gel becomes strong, with $G' > 10^4$ Pa and characterized by an interlamellar distance below ~15 nm, in agreement with a lamellar hydrogel prepared from the same compound by simple pH adjustement.[22] The gelation of G-C18:0 samples result from a defectuous lamellar phase and interfacial rearrangements leading to a local arrest, which is sufficient to provide stress-bearing properties.

Rheo-SAXS shows that the sol-to-gel process is characterized by a micelle-to-lamellar transition, as found before under dilute conditions.[35] The hydrogel formation is a dynamic process passing through the assessment of the interlayer distance, dominated by d_w (rather than the lipid layer thickness), of which the fall below ~15 nm is strongly correlated to the improvement of the mechanical properties, as seen both in the direct preparation of the gel[22] and after the sol-to-gel transition (**Figure 3b**). The origin of such oscillatory evolution of d_w is however unclear. Luzzati *et al*. have observed that concentration has a role in the unpredictable variation (cit., "*évolution apparemment capricieuse*") of the lamellar period in the lamellar region of the phase diagram of sodium and potassium salts of saturated fatty acids.[51] ^{1}H NMR experiments performed in this work during the sol-to-gel transition testify a continuous evolution of the lipid concentration in the lamellar phase. In the process of extrapolating their observations to our work, one can then formulate the hypothesis that oscillation of *d* depends on concentration fluctuations during gel formation. The interlamellar spacing in the present system is controlled by electrostatic repulsion coming from the negatigvely-charged carboxylate groups in the membrane;[22] for this reason, a fluctuating evolution of the negatively-charged G-C18:0 during acidification could be responsible for

fluctuations in the membrane surface charge density and, consequently, of fluctuating repulsive electrostatic forces.[52]

In a second hypothesis, one could evoke possible local fluctuations of ions at the membrane surface, as observed in charged phospholipid lamellar phases.[53] This phenomenon was shown to be important for divalent ions but also possible, at a smaller extent, for monovalent ions. Electrostatic repulsion forces are strongly sensitive to charge screening and variations in the local concentration of ions at the lipid membrane could certainly explain the observed variation of *d*-spacing.

Finally, variations in the osmotic pressure between the lamellar domains and the bulk solution could also explain a variable *d*-spacing. G-C18:0 hydrogels were shown to be a biphasic system where *d*-spacing is not ideal under dilute conditions.[22] Raviv *et al*. have explained by osmotic pressure arguments related to the coexistance of a disordered phase the non-ideal behaviour of *d*-spacing in dilute charged lipid membranes.[54] Similarly, one could explain the fluctuating behaviour of *d*-spacing in the present system by the evolution of the osmotic pressure applied to the lamellar domains by the outer water phase.

Effect of temperature. Shear and fast heating above the T_m were previously employed to anneal the G-C18:0 lamellar gel and allow comparable rheology experiments so to avoid samples history effects.[22] To decorrelate the combined effects of temperature and shear, we study hereafter the effect of temperature on the mechano-structural properties of a G-C18:0 gel by *in-situ* rheo-SAXS experiments. In **Figure 5c** we quantify about one order of magnitude the loss in terms of the plateau elastic modulus of a typical G-C18:0 lamellar hydrogel recorded between 25°C and 70°C (C= 5 wt%, G' at plateau ~ 10^4 Pa before heating). When temperature is decreased again to 25°C, the hydrogel recovers most of its mechanical properties after an equilibration time of 30 min to 60 min. Interestingly, temperature,

differently than pH, does not induce a gel-to-sol transition in the 25°C-70°C range, because $G' > G''$ (at ω= 6.28 rad.s^{-1}, γ= 0.1%) even at 70°C, with G' still being in the kPa range. To better understand the elastic properties of the hydrogel upon heating, we have looked at its concomitant structural properties.

In-situ rheo-SAXS experiments are shown in **Figure 5a**, where numbered (1 to 6) profile corresponds to a given temperature, of which the elastic properties are given in **Figure 5c**. The SAXS scattering profile of the G-C18:0 hydrogel at 70°C (label 4, **Figure 5a**) is very similar to the profiles recorded at 25°C (labels 1 and 6, **Figure 5a**), indicating that the lipid membrane structure is not sensitively affected by temperature. However, the evolution of *d*-spacing and full width at half maximum (FWHM) for the low-*q p1*-labeled peak with temperature, presented in **Figure 5b**, indicate that the long-range lamellar order is partially affected. When temperature reaches 70°C, the peak starts to broaden (label 3, **Figure 5a,b**) and the FWHM increases by a factor 1.5 after 20 min at 70°C (label 4, **Figure 5a,b**). As soon as the temperature is reduced (label 5, **Figure 5a,b**), the FWHM decreases to reach its original value of 0.075 nm^{-1} (label 6, **Figure 5a,b**). The noticeable inertia occurring between the moment when temperature stabilizes at 70°C (label 3, **Figure 5b**) and the peak broadening (label 4, **Figure 5b**), quantified to about 10 to 15 min, can be probably explained by the restricted diffusivity in the medium due to the strong viscosity of the hydrogel (G' > 10^4 Pa). The "bell-shaped" FWHM (**Figure 5b**) and "U-shaped" G',G'' (**Figure 5c**) profiles indicate the reversibility of the heating-cooling process on the mechano-structural properties of the G-C18:0 lamellar hydrogels.

It could be tempting to determine the number of lipid layer stacking within each lamellar domain. Given the peak position and its broadening, one can employ the Scherrer equation ($D = \frac{b2\pi}{FWHM(q)}$, b is a dimensionless constant contained between 0.89 and 0.94 and FWHM is in nm^{-1}) to estimate the size of the lamellar crystalline domains, *D*. We find *D* ~75

nm at 25°C and *D* ~50 nm at 70°C. Dividing these values by the lamellar period, we find that the lamellar domains are constituted by 4 to 6 lipid layers at 25°C and only 2 to 4 at 70°C. However, a strict calculation of the number of lipid layers should be taken with caution and these data should be rather interpreted in light of the more usual Caillé description of x-rays diffusion by smectic A phases,[55,56] where peak broadening, here at 70°C, is commonly explained by an increasing disorder of the lamellar domains due to thermal fluctuations, as reported in other similar systems.[20,57,58]

The corresponding temperature behaviour of the lamellar period, *d*, in **Figure 5b** shows an inflation of about 1.5 nm at 70°C (label 3) followed by a deflation after about ten minutes of about 2 nm. If the broadness of the peak actually makes the determination of the exact peak position a challenge, we should still observe that both increasing and decreasing of the lamellar period with increasing temperature are observed in many lipid lamellar systems. Inflation is generally explained by the presence of temperature-driven undulation long-range repulsive forces,[58–61] while deflation is explained by a contraction of the lipid hydrophobic region due melting above its T_m.[61] Concerning the possible presence of repulsive long-range undulation forces, we reasonably exclude them in this system. The actual shift of the lamellar peak of about 1.5 nm found here is not significant if compared to the typical shifts observed in other systems, generally in the order of tens[58] or even hundreds of nm.[62,63] We believe that repulsive electrostatic forces are still predominant above the T_m of the lipid. Concerning the contraction of the hydrophobic region, one cannot be excluded for variations below 0.5 nm, as found for lipid bilayers.[64] Contraction of more than 1 nm is on the contrary highly unlikely, especially considering the interdigitated nature of the lipid membrane. The small and non-linear evolution of lamellar spacing should then be explained by other phenomena occurring at the interlamellar region and involving hydration/dehydration and/or ion adsorption/desorption.[61,64]

Softening of the gel upon heating could be explained by the formation of vesicular-lamellar gels, although these are notoriously weaker gels if compared to lamellar hydrogels.[15,47,48,65] If vesiculation above the T_m cannot be totally excluded,[34] both confocal microscopy and polarized light microscopy[22] exclude the formation of onions; the latter are characterized by well-defined maltese crosses[65] under crossed polarizers and which we never observe, neither below nor above the T_m.[22] We nonetheless observe spherulitic domains of few micrometers in size, but they are composed of bent disordered lamellar sheets (**Video 1,2**, recorded at C= 2.5 wt%, pH 6 and *T*= 50°C) and rather reminiscent of a crumpled phase. The latter refers to the folding of a stiff flat system,[66] predicted theoretically in the so-called crumpling transition,[67] observed on graphene oxide sheets,[68] but only hypothesized, and never imaged (to best of our knowledge), for soft lamellar systems.[63,69] Interesting, faceted folding of G-C18:0 membranes at 70°C was already observed by cryo-TEM on diluted samples.[34]

Finally, it is not uncommon to observe a precipitate after a heating and cooling cycle. This is explained by the fact that temperature promotes condensation between lamellae, as demonstrated by the systematic and irreversible increase in the intensity of *p2*-labelled peak at q= 2.03 nm^{-1} (**Figure 5a**), corresponding to a lamellar distance of d= 2.09 nm. The FWHM of this peak is about two times smaller than the width of the low-q hump described above; the use of the Scherrer equation indicates that the lamellar domains are constituted by at least 40 to 50 lipid layers, and the Caillé interpretation indicates the formation of lamellar clusters characterized by stiffer lipid layers.

Formation of lamellar regions constituted by stiff layers when temperature is increased is unexpected and in disagreement with other lamellar system, where the opposite occurs.[58] At the moment, if we are unable to reliably explain this phenomenon, we can make several hypotheses. It is well-known that in biphasic fatty acid lamellar systems, the bulk pH does not necessarily correspond to the pH in the vicinity of the lamellae.[70,71] Temperature can then

promote diffusion of hydronium ions within the lamellar domains, thus favouring the carboxylate to carboxylic acid reaction, which reduces the surface charge density, the latter being a necessary condition to reduce electrostatic repulsion and to drive membrane collapse. However, temperature could also promote intra-membrane molecular diffusion and possible segregation in carboxylic-rich regions, thus locally reducing repulsion and inducing condensation. Other phenomena like ion diffusion could also explain charge screening effects and consequent membrane condensation, as found in other systems.[61]

In summary, in the absence of shear, temperature promotes a reversible order-disorder transition, characterized by the presence of spherulitic, crumpled, lamellar aggregates, which soften the G-C18:0 hydrogel, but without inducing a complete gel-to-sol transition. The gel can be recovered with its original elastic properties upon cooling but precipitation of dense lamellar clusters could be expected.

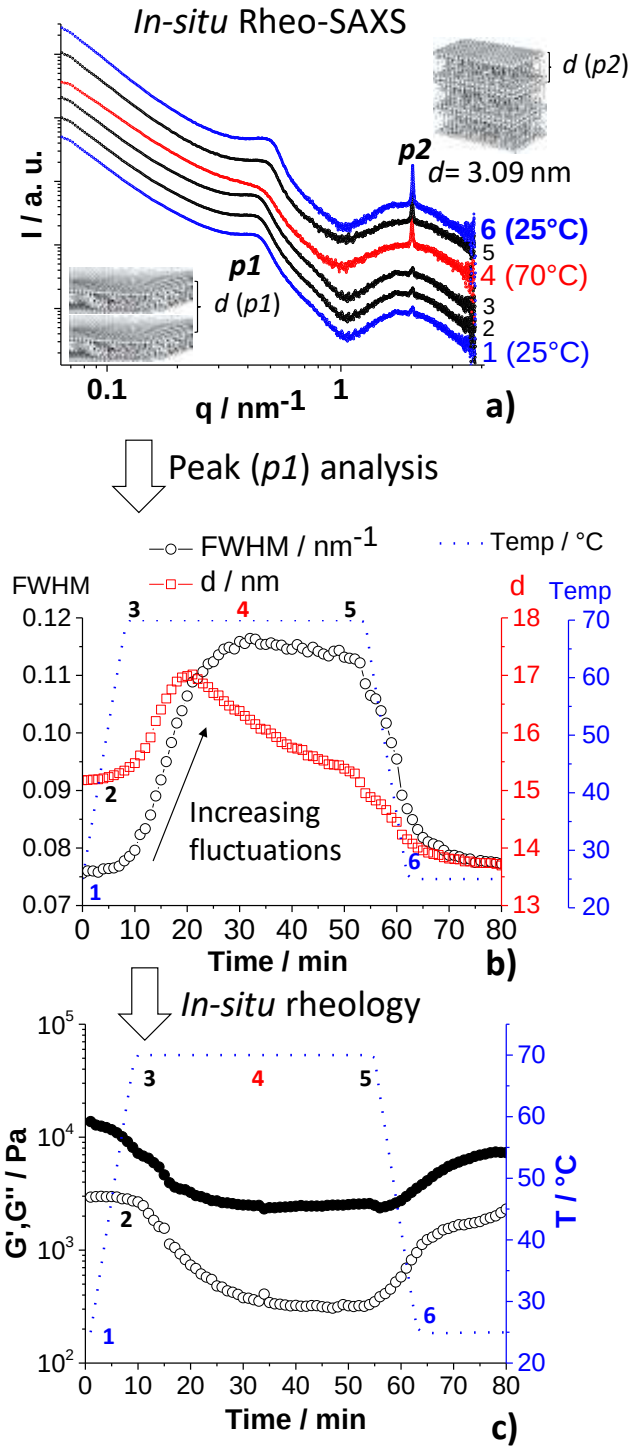

Figure 5 – a) Selected SAXS profiles collected during temperature-controlled rheo-SAXS experiments of G-C18:0 lamellar hydrogel. *d* refers to the lamellar period. Data are collected on the same sample presented in Figure 3b ($C_{G\text{-}C18:0}$= 5 wt%) after completion of GDL hydrolysis and reaching a *G'* plateau. b) Evolution with temperature of interlamellar distance of peak *p1*, *d*(*p1*), and the corresponding full width at half maximum (FWHM). c) *In-situ* rheology experiments: temperature evolution of *G´* (full

symbols) and *G´´* (open symbols) corresponding to the SAXS experiments presented in (a). Common to (b) and (c): numbers from 1 to 6 refer to the SAXS profiles in (a). Data are plot against time and the corresponding temperature profile is given by the blue dotted curve: temperature ramp of 5°C/min from 25°C to 70°C, *T*= 70°C for 60 min, then ramp to *T*= 25°C at 5°C/min.

Effect of shear. Shear is a key processing parameter when working with gels; in the specific case of lamellar phases: shear induces orientation[72] or formation of multi-lamellar vesicles (onion phase).[73,74] The shear thinning flow behavior of a lamellar phase is generally explained by the gliding of the layers relative to each other due to screw dislocations, which slide under an applied shear to counterbalance the applied vorticity,[75] or by layer tilting and dilation under shear flow, which could lead to a continuous production of dislocations.[76] Rheo-SAXS and microscopy help picturing these phenomena when shear is applied to a G-C18:0 lamellar hydrogel.

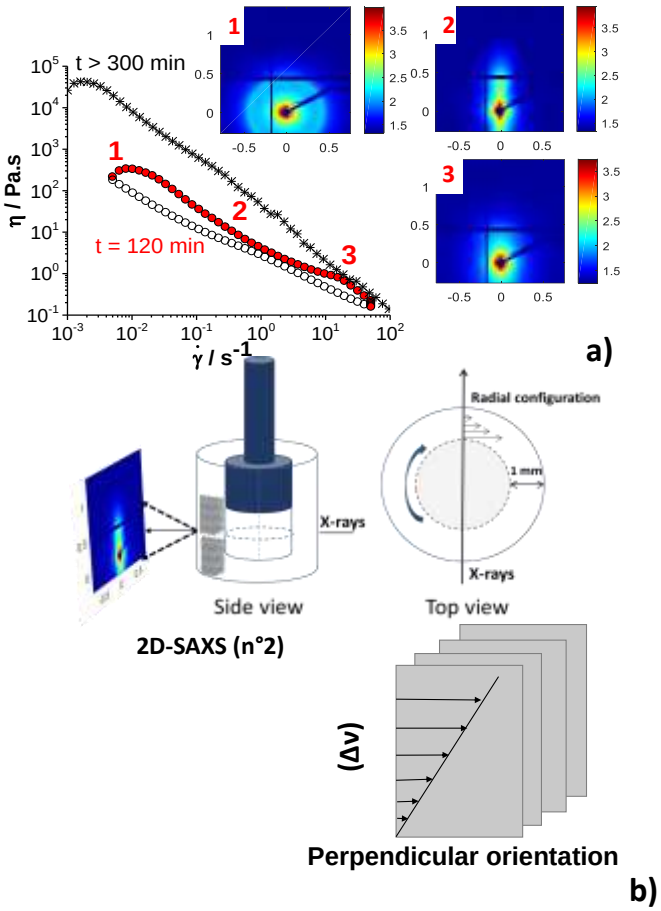

Figure 6 - a) Evolution of viscosity, η, with shear rate, $\dot{\gamma}$, recorded on the G-C18:0 hydrogel prepared in Figure 3b after 120 min (G'~ 10^2 Pa, red: ascending shear rate ramp; white: decreasing shear rate ramp) and after 300 min (G'~ 10^4 Pa, stars) at $C_{G\text{-}C18:0}$= 5 wt% (constant gap 1 mm, couette cell geometry, [GDL]= 100 mM). Images 1-3 are representative 2D SAXS patterns corresponding to 1-3 in the $\eta(\dot{\gamma})$ profile. b) Scheme representing the rheo-SAXS geometry and the perpendicular orientation from the 2D SAXS pattern n°2.

The decrease of dynamic viscosity, η, with shear rate, $\dot{\gamma}$, (**Figure 6a**) depicts a typical shear-thinning behavior of the lamellar hydrogel. $\eta(\dot{\gamma})$ profiles, recorded on G-C18:0 hydrogels prepared in **Figure 3b**, display shear-thinning properties both during (t=120 min, G'~ 10^2 Pa) and after (t>300 min, G'~ 10^4 Pa) gelation. However, after 300 min, the zero-shear plateau is two orders of magnitude higher and the shear thinning behavior is reversible (upon decreasing the shear rate, the system recovers its original viscosity). After formation of a strong gel, above t>300 min, the lamellae are isotropically oriented from zero-shear to ~10

s^{-1}, above which a mild orientation occurs up to 1000 s^{-1}, in contrast to classical orientation under shear in lamellar systems.[72,77] On the contrary, in the weak gel region below 200 min (**Figure 6a)**, lamellar orientation is more sensitive to shear: isotropic orientation at zero shear (2D SAXS pattern 1) is lost between 0.1 s^{-1} and 1 s^{-1} (2D SAXS pattern 2), where the first order Bragg reflection now clearly appears, indicating a perpendicular alignment of the lamellae with respect to the shear direction (**Figure 6b**). Between 10 s^{-1} and 100 s^{-1}, the $\eta(\dot{\gamma})$ profile is characterized by a jump (observed using plate-plate, cone-plate and couette cell geometries) and the corresponding 2D SAXS pattern 3 shows a partial loss in the lamellar alignment, due to either a change in the orientation of the lamellae, from perpendicular to parallel, or to partial disordering. Interestingly, the 2D SAXS patterns 2 and 3 are very similar to the 2D SAXS patterns measured just before the lamellar to nematic phase transition of a lipid-surfactant-water system, a region where the lamellar phase is characterized by screw-like defects.[77] Pattern 2 is closely related to patterns h and I (Fig. 1, ref. [77]) for shear rates lower than 100 s^{-1} while pattern 3 is similar to pattern k (Fig. 1, ref. [77]), which had shown an orientational 90° flip of the lamellae, as supposed in this work. The analogy between our data and data presented in Ref. [77] strongly confirms the nature of the defects in the G-C18:0 lamellar hydrogel and described elsewhere.[22]

Optical differential interference contrast microscopy (DIC-M) and cryo-TEM performed on sheared G-C18:0 hydrogels show at two different scales the structure of the gel after shear. At the scale of several micrometers, DIC-M shows the presence of both aligned lamellae and spheroids; at the nanoscale, cryo-TEM shows that the spheroids are composed of disordered condensed lamellar domains (**Figure 7**). Interestingly, DIC-M and, above all, cryo-TEM, exclude the presence of an onion phase, classically expected in a sheared lamellar phase.[73,74] The spheroidal objects shown by the cryo-TEM rather recall a crumpled phase,[66–68]

only hypothesized before, but never visualized, for soft lamellar systems,[63,69] and in agreement with the behavior found above the T_m and described in the previous section.

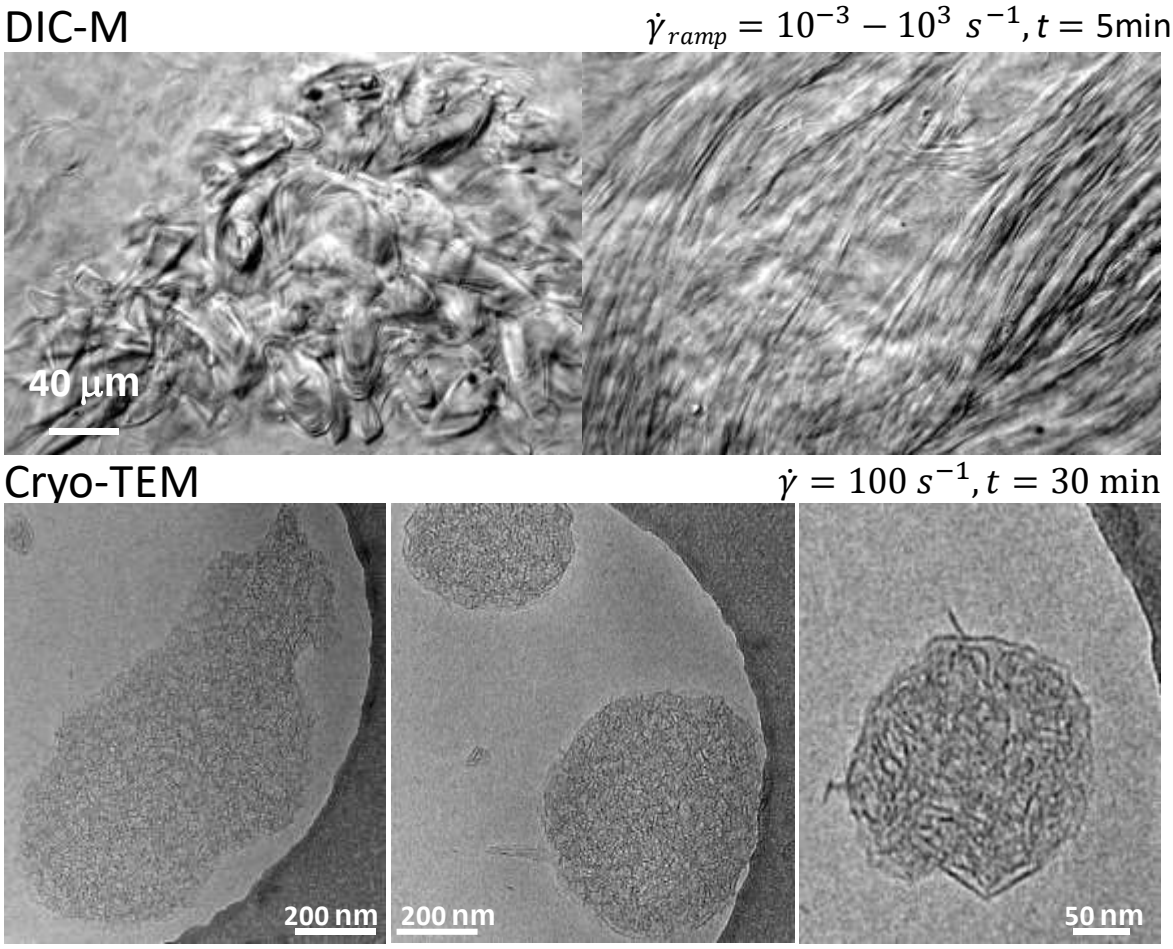

Figure 7 - DIC-M and cryo-TEM images are recorded on the lamellar hydrogel (pH~6, $C_{G\text{-}C18:0}$= 5 wt% and $C_{G\text{-}C18:0}$= 1 wt%, respectively) after shear. Shearing conditions are given on top of each set of micrographs.

In summary, rheo-SAXS combined with microscopy show a transition from lamellar to structured spheroids, possibly a crumpled phase, which, to the best of our knowledge, was never clearly reported in the literature of lipid membranes. T_m higher than RT[22] and the possible $P_{\beta,i}$ phase characterizing G-C18:0 hydrogels[22] may explain the stiffness and such unexpected behaviour under shear, instead of a lamellar-to-vesicle transition, classically obtained in L_α phases. In addition, the orientational behaviour of the G-C18:0 hydrogel under

shear confirms the presence of a defectuous (possibly screw-like defects) lamellar phase.[77]

Conclusion

This work shows the relationship between the structural and elastic properties studied by *in-situ* rheo-SAXS of a lipid lamellar hydrogel composed of a new pH-responsive glucolipid. The latter is prepared from glucose and vegetable oils from the microbial fermentation of the modified yeast *S. bombicola ΔugtB1*. Hydrogels were shown to be composed of a biphasic medium containing water and interconnected domains (100-500 μm) of kinetically-trapped lamellar phase controlled by electrostatic interactions.

pH variation from alkaline to acid at room temperature at lipid concentrations below 10 wt% induce a sol-to-gel transition, understood as a micelle-to-lamellar phase transition. The elastic properties increase after the formation of the lipid membrane, at pH below 8. The systems forms a gel with G' above 10^4 Pa for lamellar *d*-spacings below about 20 nm. Interestingly, before reaching an equilibrium value of about 15 nm corresponding to the highest elastic moduli, the *d*-spacing undergoes an unexpected oscillation, a typical sign of interlamellar dynamic attractive-repulsive forces. We attributed this unexpected feature to three possible phenomena: excess of negatively-charged glucolipids in the membrane, variation in the salt concentration at the membrane but also possible variations in the osmotic pressure between the lamellar domains and the bulk solution.

Increasing temperature above the T_m of G-C18:0 induces a partial loss in the elastic properties of the lamellar hydrogel, with *G´* still higher than *G´´* and in the order of the kPa. If this effect is generally explained in the literature by a lamellar-to-vesicle transition, *in-situ* rheo-SAXS and confocal microscopy suggest the local, although not complete, formation of spherulitic inclusions, which seem to be composed of crumpled lamellae. The same crumpled phase was detected by after submitting the lamellar hydrogel to shear rate values in the order

of 100 s^{-1} at room temperature. In this case, one classically expects a shear-induced lamellar-to-onion transition, which explains the loss in the viscosity. However, in the present system, probably due to the fact that shear is applied below the T_m, *in-situ* SAXS combined with cryo-TEM and DIC microscopy strongly suggest the formation of crumpled phase.

Acknowledgements: Experimental and technical assistance: Prof. Gijsje Koenderink and Mrs. Federica Burla (Rheo-SAXS, AMOLF Institute, Amsterdam, Netherlands). We thank Dr. S. Roelants and Prof. Wim Soetaert (Gent University, Belgium) for producing the GC18:0 compound and Dr. E. Delbeke and Prof. C. Stevens (Gent University, Belgium) for the hydrogenation reaction. Dr. O. Diat (ICSM, Marcoule, France) for helpful discussions.

Funding: European Community's Seventh Framework Programme (FP7/2007–2013) under Grant Agreement No. Biosurfing/289219; European Synchrotron Radiation Facility (ESRF), Grenoble, France, under the experiment number SC 4778; SasView application, originally developed under NSF award DMR-0520547 and funding from the European Union's Horizon 2020 (SINE2020 project, grant agreement No 654000).

Author contributions: GBM and NB performed the hydrogel experiments, analyzed the data and wrote the manuscript. PG performed cryo-TEM experiments. DHM set-up the rheo-SAXS experiments.

Competing Interests: All authors declare no conflicts of interests.

Supplementary Material: Fig. S1 and Fig. S2. Video 1 and Video 2 are downloadable at the editor's website.

References

1 G. M. Whitesides and B. A. Grzybowski, *Science (80-.).*, 2002, **295**, 2418–2421.

2 L. A. Haines, K. Rajagopal, B. Ozbas, D. A. Salick, D. J. Pochan and J. P. Schneider, *J. Am. Chem. Soc.*, 2005, **127**, 17025–17029.

3 M. R. Dreher, A. J. Simnick, K. Fischer, R. J. Smith, A. Patel, M. Schmidt and A. Chilkoti, *J. Am. Chem. Soc.*, 2008, **130**, 687–694.

4 S. Toledano, R. J. Williams, V. Jayawarna and R. V. Ulijn, *J. Am. Chem. Soc.*, 2006, **128**, 1070–1071.

5 X. Zhuang, Y. Mai, D. Wu, F. Zhang and X. Feng, *Adv. Mater.*, 2015, **27**, 403–427.

6 T. E. Wilkop, J. Sanborn, A. E. Oliver, J. M. Hanson and A. N. Parikh, *J. Am. Chem. Soc.*, 2014, **136**, 60–63.

7 M. L. Mather and P. E. Tomlins, *Regen. Med.*, 2010, **5**, 809–821.

8 A. Ainla, I. Gözen, B. Hakonen and A. Jesorka, *Sci. Rep.*, 2013, **3**, 2743.

9 M. J. Webber, E. A. Appel, E. W. Meijer and R. Langer, *Nat. Mater.*, 2015, 15, 13–26.

10 J. Israelachvili, *Intermolecular and Surface Forces*, 2011.

11 M. A. Haque, G. Kamita, T. Kurokawa, K. Tsujii and J. P. Gong, *Adv. Mater.*, 2010, **22**, 5110–5114.

12 S. R. Raghavan and J. F. Douglas, *Soft Matter*, 2012, **8**, 8539.

13 R. G. Weiss, *J. Am. Chem. Soc.*, 2014, **136**, 7519–7530.

14 J. H. Shi, X. Y. Liu, J. L. Li, C. S. Strom and H. Y. Xu, *J. Phys. Chem. B*, 2009, **113**, 4549–4554.

15 H. E. Warriner, S. H. Idziak, N. L. Slack, P. Davidson and C. R. Safinya, *Science (80-.*

)., 1996, **271**, 969–73.

16 M. Ilyas, M. A. Haque, Y. Yue, T. Kurokawa, T. Nakajima, T. Nonoyama and J. P. Gong, *Macromolecules*, 2017, **50**, 8169–8177.

17 K. Steck, J. H. van Esch, D. K. Smith and C. Stubenrauch, *Soft Matter*, 2019, **15**, 3111–3121.

18 S. Koitani, S. Dieterich, N. Preisig, K. Aramaki and C. Stubenrauch, *Langmuir*, 2017, **33**, 12171–12179.

19 J. Niu, D. Wang, H. Qin, X. Xiong, P. Tan, Y. Li, R. Liu, X. Lu, J. Wu, T. Zhang, W. Ni and J. Jin, *Nat. Commun.*, 2014, **5**, 3313.

20 C. Y. Cheng, T. Y. Wang and S. H. Tung, *Langmuir*, 2015, **31**, 13312–13320.

21 C. Stubenrauch and F. Gießelmann, *Angew. Chemie - Int. Ed.*, 2016, **55**, 3268–3275.

22 G. Ben Messaoud, P. Le Griel, S. Prévost, D. H. Merino, W. Soetaert, S. L. K. W. Roelants, C. V. Stevens and N. Baccile, *Soft Matter*, 2020, DOI: 10.1039/c9sm02158b.

23 K. M. J. Saerens, J. Zhang, L. Saey, I. N. A. Van Bogaert and W. Soetaert, *Yeast*, 2011, **28**, 279–292.

24 I. N. A. Van Bogaert, K. Saerens, C. De Muynck, D. Develter, W. Soetaert and E. J. Vandamme, *Appl. Microbiol. Biotechnol.*, 2007, 76, 23–34.

25 R. Marchant and I. M. Banat, *Trends Biotechnol.*, 2012, **30**, 558–565.

26 D. Kitamoto, T. Morita, T. Fukuoka, M. Konishi and T. Imura, *Curr. Op. Coll. Interf. Sci.*, 2009, **14**, 315–328.

27 P. Dhasaiyan and B. L. V. Prasad, *Chem. Rec.*, 2017, **17**, 597–610.

28 T. Imura, S. Yamamoto, C. Yamashita, T. Taira, H. Minamikawa, T. Morita and D. Kitamoto, *J. Oleo Sci.*, 2014, **63**, 1005–1010.

29 C. Morita, C. Kawai, A. Kikuchi, Y. Imura and T. Kawai, *J. Oleo Sci.*, 2012, **61**, 707–713.

30 G. Ben Messaoud, P. Le Griel, D. Hermida-Merino, S. L. K. W. Roelants, W. Soetaert, C. V. Stevens and N. Baccile, *Chem. Mater.*, 2019, **31**, 4817–4830.

31 N. Baccile, L. Van Renterghem, P. Le Griel, G. Ducouret, M. Brennich, V. Cristiglio, S. L. K. W. Roelants and W. Soetaert, *Soft Matter*, 2018, **14**, 7859–7872.

32 H. E. Warriner, S. L. Keller, S. H. J. Idziak, N. L. Slack, P. Davidson, J. A. Zasadzinski and C. R. Safinya, *Biophys. J.*, 1998, **75**, 272–293.

33 H. E. Warriner, P. Davidson, N. L. Slack, M. Schellhorn, P. Eiselt, S. H. J. Idziak, H. W. Schmidt and C. R. Safinya, *J. Chem. Phys.*, 1997, **107**, 3707–3722.

34 N. Baccile, M. Selmane, P. Le Griel, S. Prévost, J. Perez, C. V. Stevens, E. Delbeke, S. Zibek, M. Guenther, W. Soetaert, I. N. A. Van Bogaert and S. Roelants, *Langmuir*, 2016, **32**, 6343–6359.

35 N. Baccile, A.-S. Cuvier, S. Prévost, C. V Stevens, E. Delbeke, J. Berton, W. Soetaert, I. N. A. Van Bogaert and S. Roelants, *Langmuir*, 2016, **32**, 10881–10894.

36 G. Portale, D. Cavallo, G. C. Alfonso, D. Hermida-Merino, M. van Drongelen, L. Balzano, G. W. M. Peters, J. G. P. Goossens and W. Bras, *J. Appl. Crystallogr.*, 2013, **46**, 1681–1689.

37 W. Bras, I. P. Dolbnya, D. Detollenaere, R. van Tol, M. Malfois, G. N. Greaves, A. J. Ryan and E. Heeley, *J. Appl. Crystallogr.*, 2003, **36**, 791–794.

38 Http://www.sasview.org/docs/user/models/core_shell_bicelle.html, .

39

40 J. H. Fuhrhop, S. Svenson, C. Boettcher, E. Rössler and H. M. Vieth, *J. Am. Chem. Soc.*, 1990, **112**, 4307–4312.

41 D. J. Adams, M. F. Butler, W. J. Frith, M. Kirkland, L. Mullen and P. Sanderson, *Soft Matter*, 2009, **5**, 1856–1862.

42 J. Schindelin, I. Arganda-Carreras, E. Frise, V. Kaynig, M. Longair, T. Pietzsch, S.

Preibisch, C. Rueden, S. Saalfeld, B. Schmid, J.-Y. Tinevez, D. J. White, V. Hartenstein, K. Eliceiri, P. Tomancak and A. Cardona, *Nat. Methods*, 2012, **9**, 676–682.

43 M. C. Howland, A. W. Szmodis, B. Sanii and A. N. Parikh, *Biophys. J.*, 2007, **92**, 1306–17.

44 Y. Pocker and E. Green, *J. Am. Chem. Soc.*, 1973, **95**, 113–119.

45 D. J. Adams, L. M. Mullen, M. Berta, L. Chen and W. J. Frith, *Soft Matter*, 2010, **6**, 1971–1980.

46 B. Mao, T. Divoux and P. Snabre, *J. Rheol. (N. Y. N. Y).*, 2016, **60**, 473.

47 P. Versluis, J. C. Van de Pas and J. Mellema, *Langmuir*, 2001, **17**, 4825–4835.

48 O. Regev and F. Guillemet, *Langmuir*, 1999, 4357–4364.

49 M. Wallace, J. A. Iggo and D. J. Adams, *Soft Matter*, 2017, **13**, 1716–1727.

50 G. Feio and J. P. Cohen-Addad, *J. Polym. Sci. Part B Polym. Phys.*, 1988, **26**, 389–412.

51 F. Husson, H. Mustacchi and V. Luzzati, *Acta Crystallogr.*, 1960, **13**, 668–677.

52 T. Markovich, D. Andelman and R. Podgornik, in *Handbook of lipid membranes*, 2016, p. 3.

53 O. Szekely, A. Steiner, P. Szekely, E. Amit, R. Asor, C. Tamburu and U. Raviv, *Langmuir*, 2011, **27**, 7419–7438.

54 A. Steiner, P. Szekely, O. Szekely, T. Dvir, R. Asor, N. Yuval-Naeh, N. Keren, E. Kesselman, D. Danino, R. Resh, A. Ginsburg, V. Guralnik, E. Feldblum, C. Tamburu, M. Peres and U. Raviv, *Langmuir*, 2012, **28**, 2604–2613.

55 A. Caillé, *C. R. Hebd. Acad. Sci. Paris B*, 1972, **274**, 891.

56 F. Nallet, R. Laversanne and D. Roux, *J. Phys. II*, 1993, **3**, 487–502.

57 G. Brotons, M. Dubois, L. Belloni, I. Grillo, T. Narayanan and T. Zemb, *J. Chem. Phys.*, 2005, **123**, 024704.

58 E. Carretti, V. Mazzini, E. Fratini, M. Ambrosi, L. Dei, P. Baglioni and P. Lo Nostro, *Phys. Chem. Chem. Phys.*, 2016, **18**, 8865–8873.

59 W. Helfrich and R.-M. Servuss, *Nuovo Cim.*, 1984, **3**, 137–151.

60 W. Helfrich, *Z. Naturforsch*, 1978, **33a**, 305–315.

61 O. Lotan, L. Fink, A. Shemesh, C. Tamburu and U. Raviv, *J. Phys. Chem. A*, 2016, **120**, 3390–3396.

62 S. G. Dastidar, P. Bharath, A. Pal and V. A. Raghunathan, *Ind. Eng. Chem. Res.*, 2009, **48**, 8856–8864.

63 F. C. Larche, J. Appell, G. Porte, P. Bassereau and J. Marignan, *Phys. Rev. Lett.*, 1986, **56**, 1700–1703.

64 P. Szekely, T. Dvir, R. Aso, R. Resh, A. Steiner, O. Szekely, A. Ginsburg, J. Mosenkis, V. Guralnick, Y. Dan, T. Wolf, C. Tamburu and U. Raviv, *J. Phys. Chem. B Chem. B*, 2011, **115**, 14501–14506.

65 M. Gradzielski, *J. Phys. Condens. Matter*, 2003, **15**, R655.

66 R. Lipowsky, *Handb. Biol. Phys.*, 1995, **1**, 521–602.

67 P. Le Doussal and L. Radzihovsky, *Ann. Phys. (N. Y).*, 2018, **392**, 340–410.

68 X. Ma, M. R. Zachariah and C. D. Zangmeister, *Nano Lett.*, 2012, **12**, 486–489.

69 B. Halle and S. Gustafsson, *Phys. Rev. E*, 1997, **56**, 690–707.

70 D. P. Cistola, J. A. Hamilton, D. Jackson and D. M. Small, *Biochemistry*, 1988, **27**, 1881–1888.

71 D. P. Cistola, D. Atkinson, J. A. Hamilton and D. M. Small, *Biochemistry*, 1986, **25**, 2804–2812.

72 C. R. Safinya, E. B. Sirota, R. F. Bruinsma, C. Jeppesen, R. J. Piano and L. J. Wenzel, *Science (80-.).*, 1993, **261**, 588–591.

73 O. Diat, D. Roux and F. Nallet, *J. Phys. II Fr.*, 1993, **3**, 1427–1452.

74 A. G. Zilman and R. Granek, *Eur. Phys. J. B*, 1999, **11**, 593–608.

75 C. Meyer, S. Asnacios and M. Kléman, *Eur. Phys. J. E*, 2001, **6**, 245–253.

76 C. Y. D. Lu, P. Chen, Y. Ishii, S. Komura and T. Kato, *Eur. Phys. J. E*, 2008, **25**, 91–101.

77 O. Dhez, F. Nallet and O. Diat, *Europhys. Lett.*, 2001, **55**, 821–826.

Supplementary Information for

Effect of pH, Temperature and Shear on the Structure-Property Relationship of Lamellar Hydrogels from Microbial Glucolipids Probed by *in-situ* Rheo-SAXS

Ghazi Ben Messaoud,[1,†] Patrick Le Griel,[1] Daniel Hermida-Merino,[2] Niki Baccile[1,*]

[1] Sorbonne Université, Centre National de la Recherche Scientifique, Laboratoire de Chimie de la Matière Condensée de Paris, LCMCP, F-75005 Paris, France

[2] Netherlands Organisation for Scientific Research (NWO), DUBBLE@ESRF BP CS40220, 38043 Grenoble, France

*Correspondence to: Dr. Niki Baccile, niki.baccile@sorbonne-universite.fr, Phone: 00 33 1 44 27 56 77

† Current address: DWI- Leibniz Institute for Interactive Materials, Forckenbeckstrasse 50, 52056, Aachen, Germany

This PDF file includes:

Figs. S1 to S2

Video files

Video 1 and Video 2 are downloadable at DOI: 10.1039/c9sm02494h

Figure S 1 – Rheo-SAXS apparatus used at the BM29B beamline at ESRF synchrotron (Grenoble, France). A MCR 501 rheometer (Anton Paar, Graz, Austria) equipped with a Couette polycarbonate cell (imposed gap = 1 mm) is employed. A radial configuration is used during the Rheo-SAXS study.

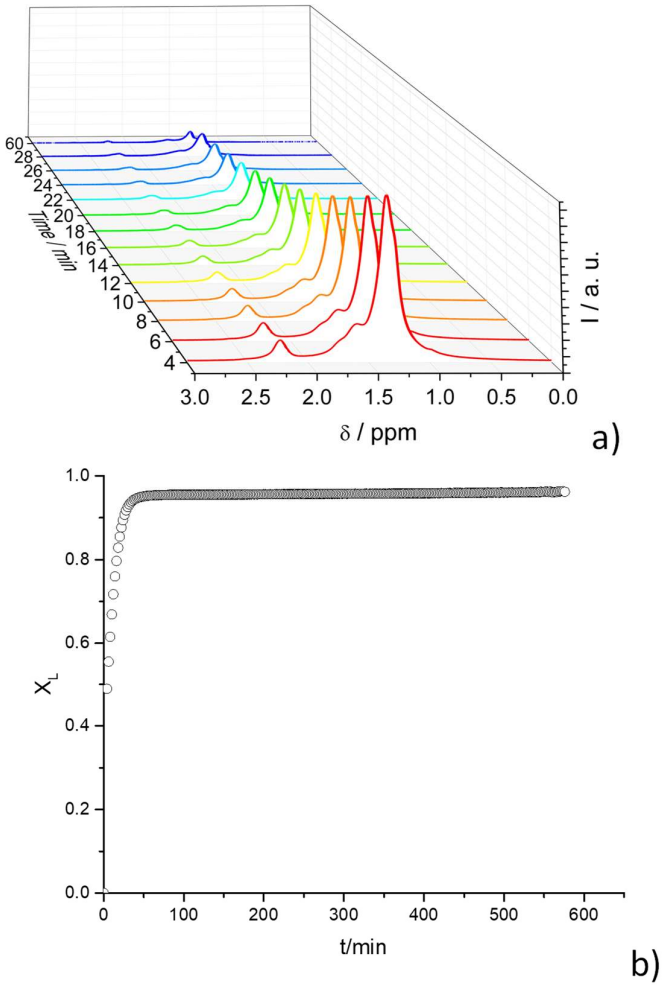

Figure S 2 – Time-resolved ^{1}H solution NMR recorded during the sol-to-gel (micellar-to-lamellar) transition of G-C18:0 glucolipid ($C_{G\text{-}C18:0}$= 5 wt%) upon acidification (initial pH 11, [GDL]= 100 mM, solvent: D_2O). a) Plot of the 1D ^{1}H NMR spectra in the 3 < δ/ppm < 0 range within one hour from GD addition. Attribution: α-CH_2, $\delta_{R\text{-}CH2\underline{CH2}COOH}$= 2.23 ppm; β-$CH_2$, $\delta_{R\text{-}\underline{CH2}CH2COOH}$= 1.61 ppm; aliphatic chain, $\delta_{\underline{R}\text{-}CH2CH2COOH}$= 1.34 ppm. b) Time evolution of the molar fraction of G-C18:0 glucolipid ($C_{G\text{-}C18:0}$= 5 wt%) in the lamellar phase X_L= 1-X_M, where X_M, the micellar fraction, is obtained by the normalized integral of the ^{1}H NMR signal of G-C18:0 in the interval 3 < δ/ppm < 0. ^{1}H NMR is only sensitive to the compound in the micellar environment.